A New Framework for Complex Wavelet Transforms

Felix C. A. Fernandes*, Rutger L. C. van Spaendonck and C. Sidney Burrus

Felix C. A. Fernandes is with the DSPS R&D Cr., Texas Instruments, Dallas, USA. E-mail: felixf@ti.com. Phone: 214-480-3257. Fax: 972-761-6966. Address: 753 Player Dr., Plano, TX 75025, USA.

Rutger L. C. van Spaendonck is with the Department of Earth Sciences, Delft University of Technology, Delft, The Netherlands. E-mail: rutger@ece.rice.edu. Phone: 31 15 2855932. Fax: 31 15 2781189.

C. Sidney Burrus is with the Department of Electrical and Computer Engineering, Rice University, Houston, USA. E-mail: csb@rice.edu. Phone: 713-348-4009. Fax: 713-348-5686.

EDICS:2-MWAV

Abstract

Although the Discrete Wavelet Transform (DWT) is a powerful tool for signal and image processing, it has three serious disadvantages: shift sensitivity, poor directionality and lack of phase information. To overcome these disadvantages, we introduce two-stage mapping-based complex wavelet transforms that consist of a mapping onto a complex function space followed by a DWT of the complex mapping. Unlike other popular transforms that also mitigate DWT shortcomings, the decoupled implementation of our transforms has two important advantages. First, the controllable redundancy of the mapping stage offers a balance between degree of shift sensitivity and transform redundancy. This allows us to create a directional, non-redundant, complex wavelet transform with potential benefits for image coding systems. To the best of our knowledge, no other complex wavelet transform is simultaneously directional and non-redundant. The second advantage of our approach is the flexibility to use *any* DWT in the transform implementation. As an example, we can exploit this flexibility to create the Complex Double-density DWT (CDDWT): a shift-insensitive, directional, complex wavelet transform with a low redundancy of $\frac{3^m-1}{2^m-1}$ in m dimensions. To the best of our knowledge, no other transform achieves all these properties at a lower redundancy.

The Discrete Wavelet Transform (DWT) provides a fast, local, sparse, multiresolution analysis of real-world signals and images. These important properties are responsible for the popularity of the DWT [1], [2], [3]. Unfortunately, the DWT also has three disadvantages that seriously undermine its application to signal- and image-processing applications. These disadvantages are shift sensitivity [4], poor directionality [5], [6] and lack of phase information [7], [8].

In the following section, we explain these disadvantages and then survey various techniques that mitigate some or all of these disadvantages simultaneously. We then motivate our mapping-based complex wavelet transforms that simultaneously overcome all three DWT disadvantages [9]. Moreover, the implementation of our complex wavelet transforms offers the additional benefits of flexibility and controllable redundancy. These benefits enable the creation of new transforms with unprecedented properties. In particular, the flexibility of our approach allows *any* DWT to have reduced shift sensitivity, improved directionality and explicit phase information. We achieve this flexibility through the implementation of our mapping-based Complex Wavelet Transform (CWT), as shown in Fig. 1. The forward CWT consists of an arbitrary DWT filter bank preceded by a mapping stage. We then invert the CWT by appending an inverse-mapping stage after an inverse-DWT filter bank. In the companion papers [9], [10], we demonstrate that this flexibility allows us to create a shift-insensitive, directional, complex wavelet transform with a

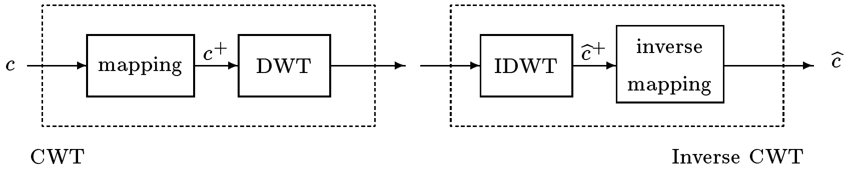

Fig. 1. The complex wavelet transform and its inverse

low redundancy factor of 2.67 in 2D. To the best of our knowledge, no other transform achieves all these properties at a lower redundancy. In addition, the controllable redundancy of the mapping stage in our complex wavelet transforms offers a balance between degree of shift sensitivity and transform redundancy. This allows us to create a directional, non-redundant, complex wavelet transform with potential benefits for image coding systems. To the best of our knowledge, no other complex wavelet transform is simultaneously directional and non-redundant.

In this paper, we shall focus on the framework of the one-dimensional, mapping-based complex wavelet transforms, their shift insensitivity and controllable redundancy. The improved directionality, explicit phase information and flexibility of these transforms are treated in greater detail in the companion papers [9], [10].

I. Mitigating DWT Disadvantages

In the previous section, we enumerated the primary disadvantages of the DWT. Several researchers have proposed different techniques to overcome these drawbacks and create a robust, informative transform for signal-processing applications. Since most methods tackle a single disadvantage, we shall group the methods according to their targeted disadvantages.

A. Reducing Shift Sensitivity

A transform is shift sensitive if an input-signal shift causes an unpredictable change in transform coefficients. Strang observed that the DWT is seriously disadvantaged by the shift sensitivity that arises from downsamplers in the DWT implementation [4]. Shift sensitivity is an undesirable property because it implies that DWT coefficients fail to distinguish between input-signal shifts.

Since downsamplers in the DWT implementation create shift-sensitivity, Mallat [11], Beylkin [12], Coifman et al. [13] and Guo et al.[14], [15] devised the undecimated DWT, a wavelet transform without downsamplers. Although the undecimated DWT is shift insensitive, it has high transform redundancy due to the absence of downsamplers. Unfortunately, the high transform redundancy incurs a massive storage requirement that makes the undecimated DWT inappropriate for most signal processing applications. As an alternative to the undecimated DWT, Liang and Parks [16], Benno and Moura [17], and Bao et al. [18] used best-basis methods or optimal wavelet-designs to reduce DWT shift-sensitivity without any increase in transform redundancy. More recently, Selesnick and Sendur [19] formulated the Double-Density Wavelet Transform (DDWT), a low-redundancy DWT extension with reduced shift sensitivity.

In 1992, Simoncelli et al. [20] confronted DWT shift sensitivity with a radically different approach. Instead of minimizing the unpredictable responses to input-signal shifts, they defined "shiftability", a new measure of reduced shift sensitivity. According to their definition, a transform is shiftable if and only if transform-subband energy is invariant under input-signal shifts. Although weaker than shift invariance, shiftability is important for applications because it is equivalent to interpolability, a property ensuring the preservation of transform-subband information under input-signal shifts. Simoncelli et al. and Wang [21] argued that since the Nyquist criterion is necessary and sufficient for shiftability, the only shiftable, non-redundant DWT is the DWT based on the Shannon wavelet. Since this particular DWT is practically unrealizable, Simoncelli et al. designed the steerable pyramid, a highly redundant, non-separable, directional, multiscale transform that attains approximate shiftability.

Abry [22] first demonstrated that approximate shiftability is possible in a DWT with a small, fixed amount of transform redundancy. He designed a pair of real wavelets such that one is approximately the Hilbert transform of the other. This wavelet pair defines a complex wavelet transform in the following sense. Consider the pair of DWT trees that implement the DWTs associated with the wavelet pair. A complex coefficient is obtained by interpreting the wavelet coefficient from one DWT tree as the real part of the complex coefficient, while the corresponding wavelet coefficient from the other tree is interpreted as the imaginary part. Magarey and Kingsbury [23], [24] showed that this complex wavelet coefficient can also be obtained using a single DWT tree based on a quasi-analytic[1] wavelet. The complex-coefficient filters that imple-

[1]Item 4 in Section III defines analytic functions.

ment this DWT have approximately half the bandwidth of the real filters associated with the DWT tree corresponding to a real-valued wavelet; consequently, the Nyquist criterion is approximately satisfied in each subband and so the DWT has approximate shiftability. However, since the quasi-analytic DWT is not an invertible transform, it can be used for analysis, but not for processing.

To overcome this disadvantage, Kingsbury [25] subsequently developed the Dual-Tree Wavelet Transform (DTWT), a quadrature pair of DWT trees similar to Abry's. Both the DTWT and Abry's transform are invertible and achieve approximate shiftability; however, the design of these quadrature wavelet-pairs is quite complicated. As an alternative, Selesnick [26], [27] recently formulated a general spectral-factorization method to design a quadrature wavelet-pair with specified length and vanishing-moment multiplicity. Gopinath generalized this design method to obtain N-tuples of wavelets in quadrature [28]. In Section IV-C, we prove that one of our mapping-based complex wavelet transforms achieves approximate shiftability at the same redundancy as the DTWT. Then in [9, Chapter 6], [10] we demonstrate that the Complex Double-Density Discrete Wavelet Transform (CDDWT), another mapping-based complex wavelet transform, enjoys reduced shift sensitivity at lower redundancy than the DTWT.

B. Improving Directionality

An m-dimensional transform suffers poor directionality when the transform coefficients reveal only a few feature orientations in the spatial domain. Since the separable 2D DWT partitions the frequency domain into three directional subbands, it enables distinction between only three spatial-domain feature orientations: horizontal, vertical and diagonal. Natural images are comprised of smooth regions that are punctuated with edges at several different orientations; consequently, poor directionality compromises the optimality of the DWT representation of natural images. Non-separable multi-dimensional filter banks have been used to obtain excellent directionality because they can partition the frequency domain optimally. Notable examples are Bamberger and Smith's directional filter bank [29] and the curvelet transforms of Donoho and Candès [30], [31] and Do and Vetterli [32]. However, to avoid complicated, non-separable filter design, Watson [5] and Burns [6] showed that filter banks with separable, analytic filters can also provide transforms with improved directionality. The DTWT of the previous subsection uses a similar technique to provide complex wavelet coefficients with improved directionality. In the companion papers [9, Chapter 5],[10], we extend our mapping-based, complex wavelet tranforms to M dimensions and then show that they also have improved directionality.

C. Providing Phase Information

In their seminal papers on wavelet transforms [7], [8], Grossman et al. claimed that they were motivated to develop the continuous wavelet transform because traditional Gabor analysis is incapable of decomposing functions using Hardy-space[2] atoms. Such a decomposition provides phase information that greatly benefits signal-processing applications. Unfortunately, most DWT implementations now use filters associated with real-valued wavelets. Consequently, signal-processing algorithms are deprived of the significant benefits of phase information. However, the DTWT and the steerable pyramid are two multiresolution decompositions that do provide phase information.

The phase information in the DTWT is associated with a quasi-analytic wavelet decomposition and has been exploited for various image-processing applications. Romberg et al. created a Hidden Markov Tree model with the complex DTWT coefficients and performed image denoising and texture classification with the model [33], [34].

The steerable pyramid introduced in Section I-A uses nonseparable filters with real coefficients to attain approximate shiftability and improved directionality. To obtain phase information, Simoncelli et al. [20] and van Spaendonck and Baraniuk [35] created complex steerable pyramids that use analytic non-separable filters. Portilla and Simoncelli [36] developed a model that incorporated the cross-scale phase statistics of complex steerable-pyramid coefficients. This model proved useful in a texture synthesis application. Van Spaendonck and Baraniuk [35] demonstrated that the smooth envelope of the complex steerable-pyramid basis functions is useful for seismic signal processing. In Section IV, we shall prove that our complex wavelet transforms provide useful phase information that may be easily exploited for signal-processing applications.

II. Compelling Reasons for Mapping-Based, Complex Wavelet Transforms

In the previous section, we examined several different methods that overcome some of the DWT disadvantages. Two of these methods, the complex steerable pyramid and the DTWT, simultaneously overcome all three disadvantages that we enumerated earlier. We shall review these methods now and then briefly explain our mapping-based, complex wavelet transforms. These complex wavelet transforms also simultaneously overcome all the disadvantages of the

[2] Item 7 in Section III defines the Hardy space.

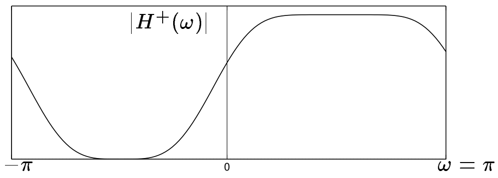

Fig. 2. $|H^+(\omega)|$, the magnitude response of the mapping filter h^+

DWT. Moreover, they also enjoy the additional benefits of flexibility and controllable redundancy.

The complex steerable pyramid is approximately shiftable, directional and provides useful phase information. Nevertheless, it is disadvantaged by high transform redundancy and the lack of perfect reconstruction in its non-separable, spatial-domain implementation. Like the complex steerable pyramid, The Dual Tree Wavelet Transform (DTWT) also simultaneously overcomes all three DWT disadvantages: shift sensitivity, poor directionality and lack of phase information. In contrast to the complex steerable pyramid, it is perfectly reconstructing and has a small fixed amount of redundancy (a factor of four in two dimensions). Nevertheless, even this small amount of redundancy makes the DTWT unsuitable for data compression, an application in which a non-redundant transform is essential. Furthermore, the DTWT can only provide an analysis using specific quadrature wavelet-pairs: it cannot be used to provide the wavelet decomposition associated with an arbitrary wavelet.

In Section I-A, we explained that the DTWT coefficients may be interpreted as arising from the DWT associated with a quasi-analytic wavelet. We now point out that there is yet another interpretation for the DTWT coefficients: they may be interpreted as the DWT of the analytic signal associated with the input signal. For an $L^2(\mathbb{R} \to \mathbb{R})$[3] input signal, the analytic signal is the Hardy-space[4] image of the input signal. Therefore, the DTWT coefficients may also be interpreted as arising from the DWT of the Hardy-space mapping of the input signal. In Section IV, we shall explain that the Hardy-space mapping of an $L^2(\mathbb{R} \to \mathbb{R})$ signal is impossible to compute. To circumvent this obstacle, we define a new function space called the Softy space. The Softy space is an approximation to Hardy space and, moreover, the Softy-space mapping of an $L^2(\mathbb{R} \to \mathbb{R})$ signal may be computed using a digital mapping filter h^+ with magnitude response shown in Fig. 2. By suppressing the negative frequencies of an input signal, h^+ maps the signal onto the Softy space which is an approximation to the Hardy space. As illustrated in

[3]Item 5 in Section III explains this notation.

[4]Item 7 in Section III defines the Hardy space and Hardy-space images.

Fig. 1, we define the CWT to be the DWT of the Softy-space mapping of an $L^2(\mathbb{R} \rightarrow \mathbb{R})$ input signal. In this paper, we shall refer to the DWT of the Softy-space mapping of an $L^2(\mathbb{R} \rightarrow \mathbb{R})$ signal as the Complex Wavelet Transform (CWT) of the signal. In [9] we demonstrate that the multi-dimensional extension of the CWT simultaneously overcomes all the enumerated DWT disadvantages: it is shiftable, directional and offers useful phase information. However, unlike the complex steerable pyramid and the DTWT, our mapping-based complex wavelet transforms have other significant benefits that we outline below.

1. *Controllable Redundancy:* The CWT consists of the DWT of the Softy-space mapping of an $L^2(\mathbb{R} \rightarrow \mathbb{R})$ signal. In Section IV, we shall show that the 1D CWT has a transform-redundancy factor of two. Note that the DTWT also has the same amount of redundancy. In Section IV-C we show that it is this redundancy that enables the DTWT and the CWT to have approximate shiftability. However, for applications such as image coding and seismic signal processing, non-redundancy is an essential property. Therefore, in Section V, we define the non-redundant mapping, an alternative to the Softy-space mapping. Unlike the Softy-space mapping, the non-redundant mapping introduces no transform redundancy although it is otherwise similar to the Softy-space mapping. We refer to the DWT of the non-redundant mapping as the non-redundant CWT. Although more shift sensitive than the CWT, the non-redundant CWT is, to the best of our knowledge, the only non-redundant, directional, complex wavelet transform[5]. This unique combination of properties implies that the non-redundant CWT has significant potential benefits for image coding systems. Hence the ability to control the redundancy of our complex wavelet transforms allows for exciting new possibilities.

2. *Flexibility:* Unlike the complex steerable pyramid and the DTWT, our complex wavelet transforms do not require the design of new wavelets. The complex wavelet coefficients are easily generated by mapping real-valued input signals onto a complex subspace and then computing the DWT of the mapping using *any* desired DWT. In [9, Chapter 6],[10] we invoke this flexibility to create the Complex Double-Density Wavelet Transform (CDDWT), a new transform based on Selesnick's Double-Density DWT [19]. This particular complex wavelet transform enjoys reduced shift sensitivity at a low redundancy factor of 2.67 in 2D. We obtained excellent results when we used the CDDWT in a seismic signal processing application [9], [10].

[5]Meyer and Coifman's brushlet transform [37] is also a non-redundant complex transform; however, it is not a wavelet transform.

In the remainder of the paper, we shall develop the framework of our complex wavelet transforms in greater detail. In Section IV, we rigorously define Softy space and the Complex Wavelet Transform (CWT). In Section IV-C, we prove that the CWT is approximately shiftable under certain conditions. Then, to demonstrate the notion of controllable redundancy, we define the non-redundant CWT in Section V. The directionality, flexibility and applications of CWTs are dealt with in the companion papers [9], [10]. Before proceeding with these sections, we present the reader with the notation and acronyms that will be employed.

III. Notation, Definitions and Acronyms

1. A function whose name begins with an upper-case letter represents the Fourier transform of the function whose name begins with the corresponding lower-case letter. For example, F denotes the Fourier transform of the function f. An infinite-length sequence of numbers will be represented by a lowercase letter. For example, c will represent an entire sequence of numbers. For some integer n, the notation $c(n)$ will denote the number indexed by n in the sequence c. The above convention for infinite-length sequences of numbers will also apply to finite-length vectors. For example, the filter-coefficient vector of an FIR filter may be represented by the lower-case letter h. The notation $h(n)$ will represent the nth element of the vector h. The Z-transform and reduced-notation Fourier transform of the vector h will be denoted by $H(z)$ and $H(\omega)$ respectively. The Z-transform of the sequence c will be denoted by $C(z)$. Recall that the evaluation of $C(z)$ on the Z-plane unit circle yields the Fourier transform denoted in standard notation as $C(e^{j\omega})$. We shall however adopt the reduced notation for the Fourier transform of a sequence and represent it by $C(\omega)$.

2. The lowercase letter j represents the imaginary unit $\sqrt{-1}$. The "*" superscript represents the complex conjugate operator. The "$_*$" subscript represents the complex conjugation of the coefficients of a Z-transform. The "$\downarrow_2$" symbol represents the operation of downsampling by a factor of two. When applied to the discrete signal x, the output of the downsampler will be represented by $\downarrow_2 x$. This signal will consist of all the even-indexed samples of x. If the downsampling factor is not mentioned, it will be assumed to be equal to two.

3. We shall denote the indicator function of the interval $[a, b)$ by $\chi_{[a,b)}$ defined as

$$\chi_{[a,b)}(x) = \begin{cases} 1, & \forall x \in [a, b), \\ 0, & \text{otherwise.} \end{cases}$$

4. *Analytic* functions have Fourier transforms that vanish over negative frequencies.

5. Usually, the notation $L^2(\mathbb{R})$ represents the space of square-integrable, complex-valued functions on the real line. To differentiate between complex-valued and real-valued functions, we shall denote this functional space by $L^2(\mathbb{R} \to \mathbb{C})$ and we shall use the notation $L^2(\mathbb{R} \to \mathbb{R})$ to represent the subspace of $L^2(\mathbb{R} \to \mathbb{C})$ that is comprised of real-valued functions. The overline denotes the closure of a set with respect to the $L^2(\mathbb{R} \to \mathbb{C})$ metric. For example, $\overline{X}$ is the closure of the set X in $L^2(\mathbb{R} \to \mathbb{C})$. If f and g are functions in $L^2(\mathbb{R} \to \mathbb{C})$, then the notation $f \approx g$ indicates that the $L^2(\mathbb{R} \to \mathbb{C})$ distance between f and g is approximately zero.

6. A *unitary* map is a linear, bijective, inner-product preserving map. Function spaces that are related through a unitary map are said to be *isomorphic* to each other. *Isometric* function spaces are related through a linear, bijective, norm-preserving map. A map is *realizable* if it may be implemented using digital filters.

7. The classical *Hardy space* $H^2(\mathbb{R} \to \mathbb{C})$ is defined by

$$H^2(\mathbb{R} \to \mathbb{C}) \stackrel{\triangle}{=} \{f \in L^2(\mathbb{R} \to \mathbb{C}) : F(\omega) = 0 \text{ for a.e. } \omega < 0\}.$$

In [9, Appendix A], Fernandes proves that $L^2(\mathbb{R} \to \mathbb{R})$ and $H^2(\mathbb{R} \to \mathbb{C})$ are isomorphic under certain conditions. Let the superscript "^{H}" denote the isomorphic *Hardy-space image* (or *Hardy-space mapping*) of an $L^2(\mathbb{R} \to \mathbb{R})$ function. Then the Hardy-space image of f is given by $F^H(\omega) \stackrel{\triangle}{=} F(\omega)\chi_{[0,\infty)}(\omega)$.

8. In this thesis, the acronym *DWT* (Discrete Wavelet Transform) will refer to Mallat's algorithm operating on the scaling coefficients of an $L^2(\mathbb{R} \to \mathbb{C})$ function. Throughout, we shall employ only real filters in Mallat's algorithm; therefore, the associated DWT wavelets and scaling functions will always be real. However since the scaling coefficients of a complex-valued $L^2(\mathbb{R} \to \mathbb{C})$ function may be complex, DWT coefficients may be complex in general. We shall use the acronym *RWT* (Real Wavelet Transform) to refer specifically to the DWT of a real-valued function in $L^2(\mathbb{R} \to \mathbb{R})$. Since we consider only DWTs implemented with real filters, RWT coefficients are always real. The acronyms *IDWT, IRWT* refer to Inverse Discrete Wavelet Transform and Inverse Real Wavelet Transform, respectively. Let h_0 be the real-coefficient scaling filter that engenders the real scaling function $\phi(x)$ in the dilation equation $\phi(x) = \sum_n h_0(n)\phi(2x - n)$. Then V_{j+1} represents the scaling space spanned by integer translates of $\phi(2^j x)$.

IV. The Complex Wavelet Transform

In this section, we motivate the definition of the CWT by explaining its reduced shift sensitivity. As described in Section I-A, to reduce shift sensitivity and storage-space requirements simultaneously, Simoncelli et al. [20] defined "shiftability", a new benchmark for shift sensitivity. The necessary and sufficient condition for shiftability is that each transform subband must satisfy the Nyquist criterion. Since RWT subband filters are non-ideal, the signal bandwidth in each RWT subband of an $L^2(\mathbb{R} \to \mathbb{R})$ function f is larger than that required by the Nyquist criterion. Hence the RWT is not shiftable.

On the other hand, if f^H is the Hardy-space image of f, then f^H has half the bandwidth of f; hence the bandwidth in each DWT subband of f^H is half the bandwidth in the corresponding RWT subband of f. Consequently the Nyquist criterion is satisfied in each DWT subband of f^H; therefore the DWT of f^H enjoys shiftability. Unfortunately, we shall now show that it is impossible to obtain f^H, the Hardy-space image of an $L^2(\mathbb{R} \to \mathbb{R})$ function, f. Let f be the projection of an $L^2(\mathbb{R} \to \mathbb{R})$ function onto the scaling space V_1 so that $f(x) = \sum_n c(n)\phi(x-n)$ or equivalently $F(\omega) = C(\omega)\Phi(\omega)$. As explained earlier, the Hardy-space image f^H is given by $F^H(\omega) = \chi_{[0,\infty)}(\omega)C(\omega)\Phi(\omega)$. Unfortunately, since $\chi_{[0,\infty)}(\omega)$ is not 2π-periodic, it cannot be applied to the scaling-coefficient sequence c using a digital filter. Since Hardy-space images of $L^2(\mathbb{R} \to \mathbb{R})$ functions are unrealizable[6] , we shall define the Softy space S^+, a practical approximation to Hardy-space. The triangle in Fig. 3 depicts the relationship between these function spaces.

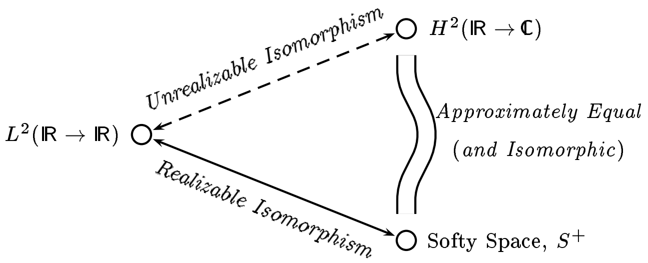

Fig. 3. Relationship between $L^2(\mathbb{R} \to \mathbb{R})$, Hardy space and Softy space.

We now define the Complex Wavelet Transform (CWT) to be the DWT of the Softy-space

[6]Realizable maps are defined in Section III, Item 6.

image of an $L^2(\mathbb{R} \to \mathbb{R})$ function, as shown in Fig. 4. The mapping-filter h^+ is used to map an $L^2(\mathbb{R} \to \mathbb{R})$ function f onto the Softy space. We then compute the DWT of the Softy-space mapping f^+ to obtain the CWT coefficients that will undergo application-specific processing. After the IDWT, an inverse-mapping filter g^+ computes the $L^2(\mathbb{R} \to \mathbb{R})$ processed function $\hat{f}$, as explained in Section IV-A. Since $f^+ \approx f^H$, the CWT will have approximate shiftability: the

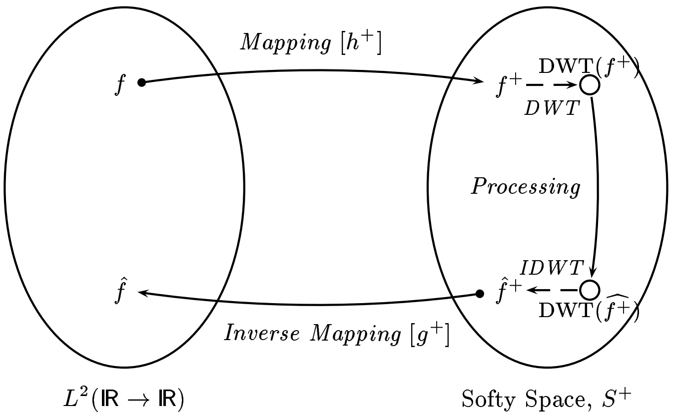

Fig. 4. f^+ is the Softy-space mapping of f. DWT(f^+) is the Complex Wavelet Transform (CWT) of f.

subband energy in DWT(f^+) will remain approximately constant under shifts of f. We prove this result in Section IV-C. Explicit phase information is available in the CWT because f^+ is a complex-valued function and therefore its DWT has complex wavelet coefficients. We explain the usefulness of this phase information and the improved directionality of the multi-dimensional CWT in [9], [10]. In this section, we first introduce the digital filters that are used to implement the realizable isomorphism between $L^2(\mathbb{R} \to \mathbb{R})$ and the Softy space. We shall then formally define the Softy space and examine its properties. These properties justify the relationships in Fig. 3 and therefore motivate the CWT definition in Fig. 4. We conclude the section with a proof for the approximate shiftability of the CWT.

A. Mapping Filters and Inverse-Mapping Filters

Proposition 1: Let h_0 and g_0 be the lowpass analysis and synthesis filters of a two-band, real-coefficient, perfect-reconstruction filter bank. Create the mapping and inverse-mapping filters

h^+ and g^+ by frequency shifting $H_0(\omega)$ and $G_0(\omega)$ by $\pi/2$, so that

$$H^+(z) = H_0(-jz), \tag{1}$$

$$G^+(z) = G_0(-jz). \tag{2}$$

Let the real scaling-coefficient sequence c be associated with a function f in V_1. The "mapping" block in Figure 5 illustrates the forward map to the scaling-coefficient sequence c^+ associated with $f^+ \in V_1^+$, the image of f where

$$\begin{aligned} V_1^+ \triangleq & \{f^+ : \forall f \in V_1, \text{where } F(\omega) = C(\omega)\Phi(\omega), \\ & \text{define } C^+(\omega) = H^+(\omega)C(\omega), \\ & F^+(\omega) = C^+(\omega)\Phi(\omega)\}. \end{aligned}$$

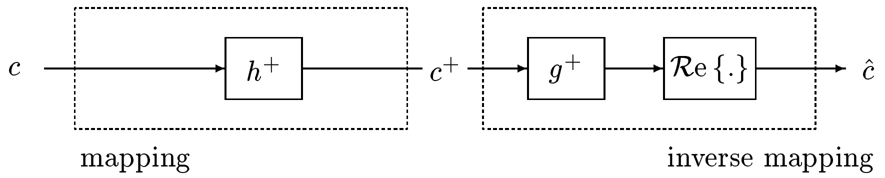

Fig. 5. The projection and its inverse constitute a realizable bijective map because $\hat{c} = c$.

The "inverse mapping" block shows the inverse map from c^+ to $\hat{c}$. Then we have $\hat{c} = c$.

Proof: Let the subscript "$_*$" denote complex conjugation of the Z-transform coefficients. Then since the real part of a complex number may be obtained by the addition of its complex conjugate, we have

$$\begin{aligned} \hat{C}(z) &= G^+(z)H^+(z)C(z) + G_*^+(z)H_*^+(z)C_*(z), \\ &= [G^+(z)H^+(z) + G_*^+(z)H_*^+(z)]C(z), \\ & \quad \text{since } c \text{ is real}, \\ &= [G_0(\nu)H_0(\nu) + G_0(-\nu)H_0(-\nu)]C(j\nu), \\ & \quad \text{where } \nu = -jz, \\ &= C(z), \quad \text{since } G_0(\nu)H_0(\nu) \text{ is a halfband filter.} \quad \square \end{aligned}$$

Proposition 1 demonstrates that the linear, bijective map between V_1 and V_1^+ is realizable because it is implementable with the digital filters h^+, g^+. We now show that this concept extends easily from V_1 to V_k, $\forall k \in \mathbb{Z}$. Given $f \in V_k$, the filter $H^+(2^{k-1}\omega)$ defines a new function space V_k^+:

$$\begin{aligned} V_k^+ \;\stackrel{\triangle}{=}\; & \{f^+ : \forall f \in V_k, \text{where } F(\omega) = C(2^{k-1}\omega)\Phi(2^{k-1}\omega), \\ & \text{define } C^+(\omega) = H^+(2^{k-1}\omega)C(2^{k-1}\omega), \\ & F^+(\omega) = C^+(\omega)\Phi(2^{k-1}\omega)\}, \forall k \in \mathbb{Z}. \end{aligned} \tag{3}$$

In Proposition 1, if we use the filters $H^+(2^{k-1}\omega), G^+(2^{k-1}\omega)$ instead of $H(\omega), G(\omega)$ respectively, then we obtain an implementation of the linear, bijective map between V_k and V_k^+.

The filter h^+ introduced in Proposition 1 is called a "mapping" filter because it enables the mapping of functions from V_k onto V_k^+. Since h^+ is a complex-coefficient filter, it introduces a redundancy factor of two when applied to a real-valued scaling-coefficient sequence. We call g^+ the "inverse-mapping" filter because it accomplishes the inverse mapping from V_k^+ to V_k. From the implementation perspective in Fig. 1, the CWT consists of the mapping block in Fig. 5 followed by a filter bank for Mallat's DWT algorithm. The mapping filter h^+ has the typical magnitude response shown in Fig. 2. The inverse CWT consists of the corresponding IDWT filter bank followed by the inverse-mapping block in Fig. 5. We are now ready to define the Softy Space formally.

B. *The Softy Space*

Definition 1: Let $V_k,\ k \in \mathbb{Z}$ be the sequence of real, nested scaling spaces associated with a real, scaling filter h_0 of length M. Suppose that h^+ is the length-N mapping filter described in Proposition 1. As proved in [9], the mapping filter h^+ unitarily maps real scaling-coefficient sequences associated with functions in V_k onto complex scaling-coefficient sequences associated with functions in the function space V_k^+, $\forall k \in \mathbb{Z}$. We define the **Softy space $\mathbf{S}^+$** associated with h_0 and h^+ as

$$S_{M,N}^+ \stackrel{\triangle}{=} \overline{\cup_{k\in\mathbb{Z}} V_k^+}. \tag{4}$$

We wish to stress that the preceding definition creates a *family* of function spaces parameterized by scaling and mapping filters of lengths M and N respectively. On selecting specific scaling and mapping filters of lengths M_0 and N_0, we define the Softy space S_{M_0,N_0}^+ associated with these particular filters. For brevity, we will sometimes omit the subscripts in this notation and write

S^+; this notation still refers to the Softy space associated with specific scaling and mapping filters that are determined from the context.

In [9], we prove several results that justify the relationships between the function spaces in Fig. 3. We list some of those results here.

1. $L^2(\mathbb{R} \to \mathbb{R})$, $H^2(\mathbb{R} \to \mathbb{C})$ and S^+ are isometric to each other with respect to the usual $L^2(\mathbb{R} \to \mathbb{C})$ inner product. Note that these function spaces are *not* isomorphic to each other with respect to this inner product because Hardy-space mappings and Softy-space mappings fail to preserve the $L^2(\mathbb{R} \to \mathbb{C})$ inner product. Fortunately, an equivalent definition of the inner product for real functions leads to isomorphisms as explained in the following result.

2. Suppose that f, g are arbitrary $L^2(\mathbb{R} \to \mathbb{C})$ functions. Define the Softy-space inner product to be the real part of the $L^2(\mathbb{R} \to \mathbb{C})$ inner product,

$$\langle f, g\rangle_+ \triangleq \mathcal{R}e\left\{\int_{-\infty}^{\infty} f(x)g(x)^* dx\right\}, \ \forall f, g \in L^2(\mathbb{R} \to \mathbb{C}). \tag{5}$$

Then $L^2(\mathbb{R} \to \mathbb{R})$, $H^2(\mathbb{R} \to \mathbb{C})$ and S^+ are isomorphic to each other with respect to the Softy-space inner product over real-valued scalars[7]. [9]. This result justifies the isomorphisms in Fig. 3. Observe that the Softy-space inner product is equivalent to the usual $L^2(\mathbb{R} \to \mathbb{C})$ inner product for the real-valued functions that comprise $L^2(\mathbb{R} \to \mathbb{R})$. Therefore the the isomorphism between $L^2(\mathbb{R} \to \mathbb{R})$ and S^+ is important because it allows the CWT to be an orthogonal (inner-product preserving) transform if an orthogonal DWT is used to compute $DWT(f^+)$ in Fig. 4. Orthogonality is an important requirement in many transform-based signal-processing applications.

3. Let h_M^+ be the length-M equiripple lowpass filter that is associated with the Softy space $S_{M,N}^+$. Then $\forall f \in L^2(\mathbb{R} \to \mathbb{R})$, let f^H and f^+ denote the images of f in $H^2(\mathbb{R} \to \mathbb{C})$ and $S_{M,N}^+$ respectively. According to [9], we have

$$||f^H - f^+||_2^2 \sim \begin{cases} O(M^{-1}), & \text{for fixed } N, \\ O(N^{-1}), & \text{for fixed } M. \end{cases}$$

This result demonstrates that the approximation of Softy-space to Hardy space improves asymptotically in the lengths of the scaling and mapping filters. The result justifies the approximation of S^+ to $H^2(\mathbb{R} \to \mathbb{C})$ in Fig. 3. Fundamentally, this approximation is realized because the mapping filter h^+, defined in Proposition 1, suppresses negative frequencies as shown in Fig. 2. To

[7]Note that the Softy-space inner product is not a valid inner product over complex-valued scalars.

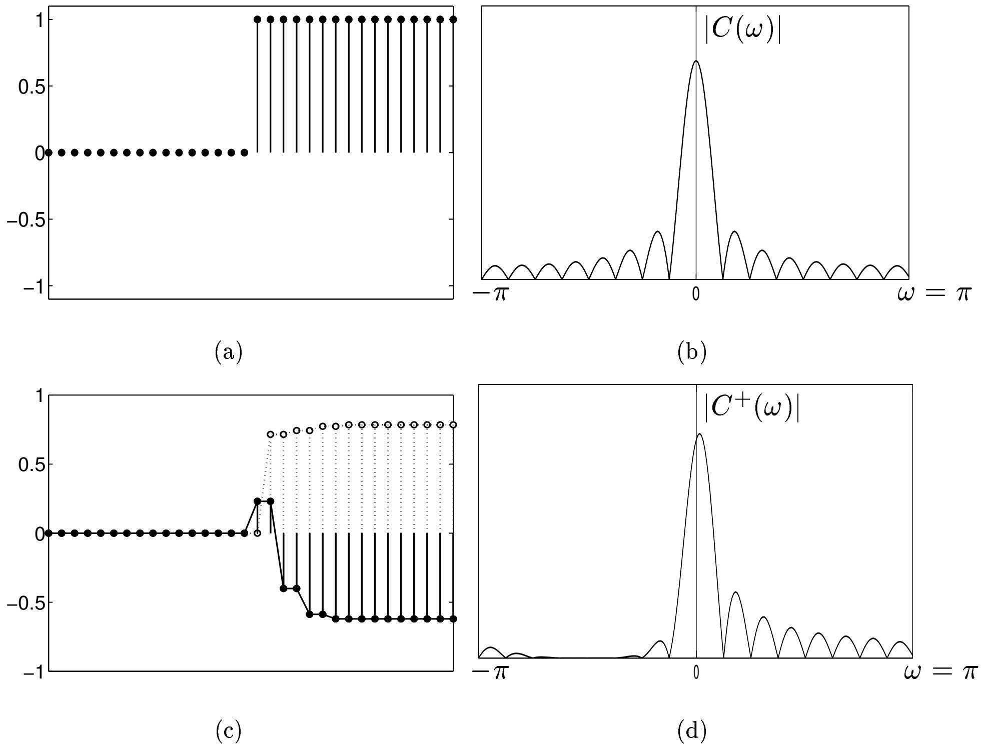

Fig. 6. (a) The step scaling-coefficient sequence c, (b) $|C(\omega)|$, the magnitude-Fourier transform of c, (c) c^+, the Softy-space mapping of c (solid circles represent the real part, hollow circles represent the imaginary part), (d) $|C^+(\omega)|$, the magnitude-Fourier transform of c^+.

illustrate the approximation, in Figs. 6(a) and 6(b) we plot c, the scaling-coefficient sequence of a step function and $|C(\omega)|$, the magnitude-Fourier transform of c. Then in Fig. 6(c), we show the Softy-space mapping c^+ obtained by passing c through the mapping filter h_8^+. The magnitude-Fourier transform $|C^+(\omega)|$, of this mapping is depicted in Fig. 6(d). Clearly, the negative frequencies of $C^+(\omega)$ in Fig. 6(d) are suppressed when compared to the negative frequencies of $C(\omega)$ in Fig. 6(b). Recall that the negative frequencies of Hardy-space functions are identically zero. Therefore, this illustrates the approximation of Softy space to Hardy space. It also ensures that the CWT is approximately shiftable, as shown in the following section.

C. Shiftability of the CWT

To prove that the CWT is shiftable, we must show that CWT subband energy is approximately constant under input-signal shifts. Recall that the CWT filter-bank implementation consists of a DWT filter bank preceded by the mapping filter h^+.

For a Level-M DWT, the lowpass subband is as shown in Fig. 7. It consists of M iterations of the scaling filter $H_0(\omega)$ and downsampler. Define the filter $H_l^M(\omega)$ by

$$H_l^M(\omega) \triangleq H_0(\omega)H_0(2\omega)\dots H_0(2^{M-1}\omega),\ M \geq 1, \tag{6}$$

so that we may exploit the Noble identity to represent the lowpass subband by the filter $H_l^M(\omega)$ followed by a downsampler with decimation factor 2^M as shown in Fig. 8.

In the next proposition, we prove that the CWT will have approximate shiftability provided that sufficiently long filters are used in the implementation. To prove this result we need explicit characterizations for the stopbands of the scaling and wavelet filters. Hence we shall assume that Daubechies scaling and wavelet filters are used to compute the DWT. Note that the proposition will hold in general for arbitrary scaling and wavelet filters. The critical scaling-filter length for shiftability will be determined by the mapping filter's transition bandwidth δ_+[8]: shorter bandwidths imply that shiftability is possible with shorter scaling filters.

Proposition 1: Let $H^+(\omega)$ be a mapping filter with a transition bandwidth of δ_+. Consider the CWT implemented by placing $H^+(\omega)$ before an M-level DWT that uses Daubechies scaling and wavelet filters of length $N+1$. This CWT has approximate shiftability if $N \geq 15$ and

$$\frac{8}{\sqrt{N}} + 2^M \delta_+ \leq 2\pi. \tag{7}$$

Proof:

Let x^+ be the Softy-space image of x, an $L^2(\mathbb{R} \to \mathbb{R})$ function. If c^+ and c are the scaling-coefficient sequences associated with x^+ and x, then $C^+(\omega) = H^+(\omega)C(\omega)$. The level-$M$ CWT lowpass subband is shown in Fig. 9.

[8] δ_+ denotes the interval over which the mapping filter transitions from the passband to the stopband. We measure δ_+ as the frequency range over which the mapping filter's magnitude response drops from 98% of its maximum value to 2% of its maximum value.

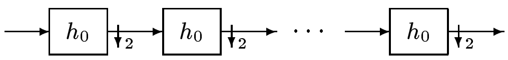

Fig. 7. The Level-M DWT lowpass subband consists of M iterations of the scaling filter and downsampler.

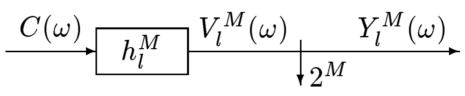

Fig. 8. Level-M lowpass subband expressed using the Noble identity.

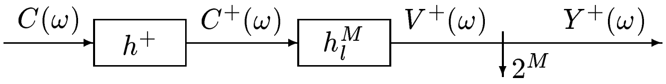

Fig. 9. Level-M CWT lowpass subband consists of a mapping filter followed by the Level-M lowpass subband.

The filtered output will be labeled v^+ and the subband output after downsampling will be denoted by y^+. We have

$$Y^+(\omega) = \sum_{m=0}^{2^M-1} V^+\left(\frac{\omega - 2\pi m}{2^M}\right),$$

where

$$V^+(\omega) = H_l^M(\omega) C^+(\omega). \tag{8}$$

We now wish to study the effect of an input-signal shift on subband energy. We shall consider only integer-shifts of the input signal x. Shifting x by an integer k causes the scaling-coefficient sequence $c(n)$, $\forall n \in \mathbb{Z}$ to shift to $c(n-k), \forall n \in \mathbb{Z}$. In response to this shift, the scaling-coefficient spectrum $C(\omega)$ will become $C(\omega)e^{jk\omega}$, denoted by $C_k(\omega)$. The scaling-coefficient spectrum $C^+(\omega)$ changes to $C_k^+(\omega) = C^+(\omega)e^{jk\omega}$, the filtered output $V^+(\omega)$ changes to $V_k^+(\omega) = V^+(\omega)e^{jk\omega}$ and $Y^+(\omega)$ changes to

$$Y_k^+(\omega) = \sum_{m=0}^{2^M-1} V^+\left(\frac{\omega - 2\pi m}{2^M}\right) e^{jk\frac{\omega - 2\pi m}{2^M}}.$$

The L^2-energy of $Y_k^+(\omega)$ is $||y_k^+||_2^2 = \int_{-2^M\pi}^{2^M\pi} |Y_k^+(\omega)|^2 d\omega$. This implies that

$$\begin{aligned} 2^M ||y_k^+||_2^2 &= \int_{-2^M\pi}^{2^M\pi} \left(\sum_{m=0}^{2^M-1} \left| V^+\left(\omega - \frac{2\pi m}{2^M}\right)\right|^2 + \right. \\ &\qquad \left. 2 \sum_{m,n=0; m\neq n}^{2^M-1} \Delta_{m,n}^+(k) \right) d\omega, \end{aligned} \tag{9}$$

where

$$\Delta_{m,n}^+(k) \triangleq \mathcal{R}\mathrm{e}\left\{ V^+\left(\omega - \frac{2\pi m}{2^M}\right) V^+\left(\omega - \frac{2\pi n}{2^M}\right)^* e^{jk\frac{2\pi m}{2^M}(n-m)} \right\}.$$

Finally, in [9] we prove that $\Delta_{m,n}^+(k) \approx 0, \forall m, n \in \{0, \ldots, 2^M-1\}$ if $N \geq 15$ and $\frac{8}{\sqrt{N}} + 2^M\delta_+ \leq 2\pi$. Hence Equation 9 implies that

$$2^M ||y_k^+||_2^2 \approx \int_{-2^M\pi}^{2^M\pi} \sum_{m=0}^{2^M-1} \left| V^+\left(\omega - \frac{2\pi m}{2^M}\right)\right|^2 d\omega.$$

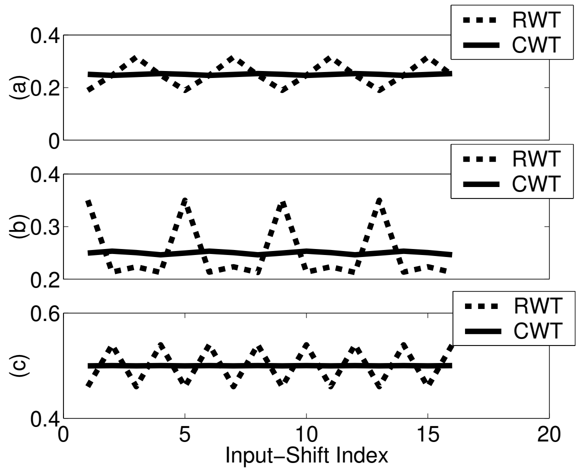

Fig. 10. Subband-energy\input-shift for RWT and CWT subbands. (a) Level-2 lowpass subband-energy, (b) Level-2 bandpass subband-energy, (c) Level-1 bandpass subband-energy. Both the RWT and CWT used length-16 Daubechies scaling and wavelet filters. The CWT mapping filter was generated from a length-16 Daubechies scaling filter.

Since the subband-energy $||y_k^+||_2^2$ is almost constant with respect to an input shift k, the Level-M CWT lowpass subband has approximate shiftability. Similarly we can prove that the Level-M CWT bandpass subband-energy is approximately preserved under input-signal shifts. Hence the CWT has approximate shiftability if $N \geq 15$ and Condition 7 holds. $\square$

To corroborate our proof for approximate shiftability of the CWT, we now provide experimental evidence for this property. We fed an impulse signal to a two-level RWT and also to a two-level CWT. Then for both transforms we computed the subband energy over 16 circular shifts of the input signal. Fig. 10 shows the transform-subband energies as a function of input-signal shifts. Observe the large oscillations in the RWT subband energies. In contrast, the CWT subband energy remains approximately constant over input-signal shifts. This corroborates our proof for approximate shiftability of the CWT.

V. The Non-Redundant CWT

In the preceding section, we introduced the CWT as the DWT of f^+, the Softy-space mapping of an $L^2(\mathbb{R} \rightarrow \mathbb{R})$ function f. Since f^+ approximates f^H, the Hardy-space mapping of f, the CWT exhibits explicit phase information, reduced shift sensitivity and improved directionality. These advantages are obtained at the expense of a small amount of data redundancy introduced by the mapping filter. However, redundancy is unacceptable in applications such as data compression. Therefore, in this section we shall first develop the non-redundant mapping: a mapping that incurs no data redundancy while mapping an $L^2(\mathbb{R} \to \mathbb{R})$ function onto a function space that approximates Softy space. We shall refer to the DWT of the non-redundant mapping of an $L^2(\mathbb{R} \to \mathbb{R})$ function as "the non-redundant CWT". The ability to control the redundancy of our mapping-based complex wavelet transforms by choosing between the Softy-space mapping and the non-redundant mapping is a unique advantage of these transforms. In Section V-A, we define the non-redundant mapping and then relate it to the Softy-space mapping in Section V-B. This relationship will explain why the non-redundant CWT enjoys explicit phase information and improved directionality but not reduced shift sensitivity. Hence the non-redundant CWT will benefit applications such as data compression in which a non-redundant transform is more important than reduced shift sensitivity.

Apart from creating the non-redundant CWT, the non-redundant mapping has another significant application. In the companion papers [9], [10], we demonstrate that the non-redundant mapping may be used to enhance directionality and provide useful phase information without increasing the redundancy and while preserving the shift-invariance properties of transforms such as the undecimated DWT and the Double-Density DWT [19]. This flexibility to create new transforms with unprecedented properties is another unique advantage of our mapping-based complex wavelet transforms.

A. Defining the Non-Redundant Mapping

In Section IV-B we used the mapping filter h^+ to define the Softy-space mapping of an $L^2(\mathbb{R} \to \mathbb{R})$ function. As explained in Section IV-A, the complex coefficients of h^+ introduce data redundancy into the CWT. To eliminate this data redundancy, we now propose the non-redundant mapping scheme shown in Fig. 11. As depicted in the figure, we define the non-redundant mapping to be the concatenation of a mapping filter and a downsampler (elimination of odd-indexed scaling coefficients). The downsampler eliminates the redundancy created by the mapping filter that generates complex scaling coefficients from real scaling coefficients. Observe that the scaling-coefficient sequences c and $\widetilde{c}^+$ can both be represented by N real numbers within a digital computer; therefore, there is no data redundancy in the scaling-coefficient sequence $\widetilde{c}^+$.

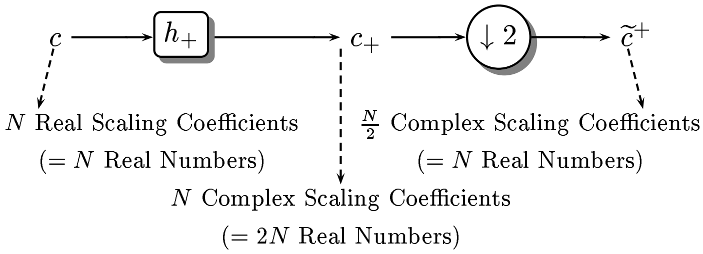

Fig. 11. The non-redundant mapping consists of a mapping filter followed by a downsampler. This mapping is non-redundant because $\widetilde{c}^+$ has the same storage requirement as c (N real numbers).

B. Relating the Non-Redundant Mapping to the Softy-Space Mapping

Given the scaling-coefficient sequence c associated with a function f in the scaling space V_1, we know that the scaling-coefficient sequence c^+ is associated with f^+ in V_1^+, where f^+ is the S^+ image of f. Our immediate task is to characterize the function space containing the functions associated with the scaling-coefficient sequences $\widetilde{c}^+$ that arise from the non-redundant mapping in Fig. 11. Let us denote that function space by $\widetilde{V}_0^+$ where

$$\begin{aligned} \widetilde{V}_0^+ \triangleq \Big\{ \widetilde{f}^+ : \widetilde{F}^+(\omega) &= \widetilde{C}^+(2\omega)\Phi(2\omega), \text{ where } \widetilde{c}^+ = \downarrow_2 c^+, \\ \text{and } C^+(\omega) &= H^+(\omega)C(\omega), \\ \text{with } F(\omega) &= C(\omega)\Phi(\omega), \forall f \in V_1 \Big\}. \end{aligned}$$

By definition, the non-redundant mapping maps V_1 onto $\widetilde{V}_0^+$. Denote this map by $\widetilde{\mathcal{H}}^+$. In Section V-C we shall prove that $\widetilde{\mathcal{H}}^+$ is a unitary map. First however, we shall use $\widetilde{\mathcal{H}}^+$ to relate $\widetilde{V}_0^+$ to the Softy space defined in Section IV-B. This relationship will enable us to exploit the non-redundant mapping to obtain some of the advantages associated with the CWT.

We shall now introduce some notation for the function spaces used to demonstrate the link between the non-redundant mapping and the Softy-space mapping. Refer to Fig. 12 for the inter-relationships between these function spaces. Let V_1^L denote the subset of lowpass functions in V_1 so that $\forall f \in V_1^L$ the scaling-coefficient sequences c associated with f satisfy the condition that $|C(\omega)|$ is small for $|\omega| \in [\pi/2, \pi)$. The function space V_1^L is mapped onto $\widetilde{\mathcal{H}}^+ V_1^L$ by the non-redundant mapping. Let us now consider the action of the DWT on V_1^L. In the multiresolution analysis that underlies the DWT, we use V_0 to denote the lower resolution scaling space obtained by filtering and downsampling scaling-coefficient sequences associated with V_1 functions. We shall

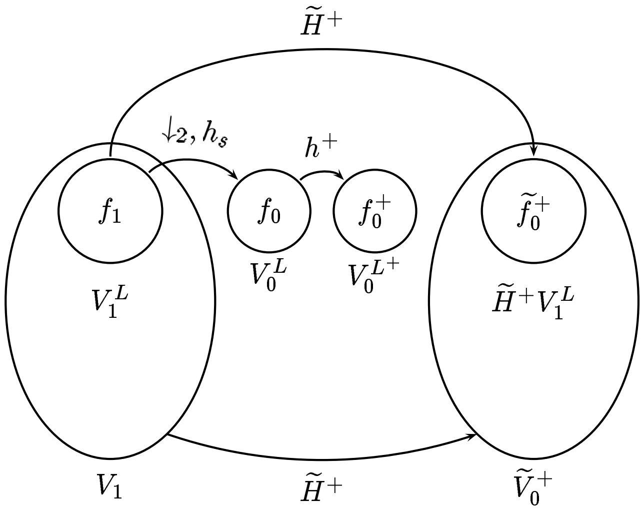

Fig. 12. The relationship between $\widetilde{H}^+$ and the Softy-Space Mapping h^+ implies that for all lowpass functions f_1, the associated functions f_0^+ and $\widetilde{f}_0^+$ are approximately equal.

now use V_0^L to denote the subset of V_0 that is obtained from V_1^L functions by the aforementioned filtering and downsampling. Let $V_0^{L^+}$ represent the function space comprised of the Softy-space images of V_0^L functions. We are now ready to demonstrate the relationship between $\widetilde{\mathcal{H}}^+V_1^L$, the non-redundant mapping of lowpass functions and $V_0^{L^+}$, a subset of the Softy space.

Proposition 2: Refer to Fig. 12. Consider an arbitrary function $f_1 \in V_1^L$, where f_1 is associated with the scaling-coefficient sequence c_1. Let f_0 denote the image of f_1 in the function space V_0^L. The function f_0 is associated with the scaling-coefficient sequence c_0 that is obtained after filtering c_1 with the scaling filter h_s and downsampling. Let f_0^+ be the Softy-space image of f_0. The function f_0^+ lies in the function space $V_0^{L^+}$, and is associated with the scaling-coefficient sequence c_0^+. Now suppose that $\widetilde{f}_0^+$ is the image of f_1 under the non-redundant mapping $\widetilde{\mathcal{H}}^+$. The function $\widetilde{f}_0^+$ belongs to the function space $\widetilde{\mathcal{H}}^+V_1^L$ and is associated with the scaling-coefficient sequence $\widetilde{c}_0^+$. Then the non-redundant mapping $\widetilde{f}_0^+$ is approximately equal to the Softy-space function f_0^+.

Proof: Refer to [9, Pg.73] for an intuitive explanation of this proof. We have

$$F_1(\omega) = C_1(\omega)\Phi(\omega), \forall\omega,$$

and

$$F_0(\omega) = C_0(2\omega)\Phi(2\omega), \forall\omega, \tag{10}$$

where c_0 and c_1 are related by

$$C_0(\omega) = C_1(\omega/2)H_s(\omega/2) + C_1(\omega/2+\pi)H_s(\omega/2+\pi), \forall\omega.$$

Since $f_1 \in V_1^L$, $|C_1(\omega)|$ is small in the range $|\omega| \in [\pi/2, \pi)$, and so $\forall\omega \in [-\pi,\pi]$, the term $C_1(\omega/2+\pi)H_s(\omega/2+\pi)$ is also small in magnitude. Hence

$$C_0(\omega) \approx C_1(\omega/2)H_s(\omega/2), \quad \forall\omega \in [-\pi,\pi].$$

Note that since $C_0(\omega)$ is still 2π-periodic, we may describe it for all ω as

$$C_0(\omega) \approx C_1\left(\frac{[\omega+\pi]\mathrm{mod}2\pi - \pi}{2}\right) H_s\left(\frac{[\omega+\pi]\mathrm{mod}2\pi - \pi}{2}\right), \forall\omega. \tag{11}$$

Now let us write $\widetilde{c}_0^+$ as,

$$\begin{aligned}
\widetilde{C}_0^+(\omega) &= C_1(\omega/2)H_+(\omega/2) + C_1(\omega/2+\pi)H_+(\omega/2+\pi), \\
&\quad \forall\omega \in [-\pi,\pi], \\
&\approx C_1(\omega/2)H_+(\omega/2), \forall\omega \in [-\pi,\pi], \\
&\quad \text{ since } C_1(\omega) \text{ has a lowpass characteristic.} \\
&\approx C_1(\omega/2)H_s(\omega/2)H^+(\omega/2), \forall\omega \in [-\pi,\pi], \\
&\quad \text{ since } H_s(\omega/2) \approx 1, \ \forall\omega \in [-\pi,\pi].
\end{aligned}$$

Since $\widetilde{C}_0^+(\omega)$ is also 2π-periodic, we may describe it for all ω by

$$\begin{aligned}
\widetilde{C}_0^+(\omega) &\approx C_1\left(\frac{[\omega+\pi]\mathrm{mod}2\pi - \pi}{2}\right) H_s\left(\frac{[\omega+\pi]\mathrm{mod}2\pi - \pi}{2}\right) \\
&\quad H^+(\omega), \forall\omega, \\
&\approx C_0(\omega)H^+(\omega), \forall\omega, \text{ from Equation 11}, \\
&= C_0^+(\omega), \ \forall\omega. \qquad (12)
\end{aligned}$$

We conclude that $\widetilde{f}_0^+ \approx f_0^+$. $\square$

We have just proved that the non-redundant mapping of an $L^2(\mathbb{R} \to \mathbb{R})$ function with a lowpass characteristic is approximately equal to the Softy-space mapping of a low resolution version of the function. This result is significant because it empowers the non-redundant mapping with some of the advantages associated with the Softy-space mapping.

Since $\widetilde{C}_0^+(\omega) \approx C_0^+(\omega)$ as proved above, we can expect the DWT of $\widetilde{C}_0^+(\omega)$ to also provide useful phase information and improved directionality [9, Chapter 5],[10]. Unfortunately the DWT of $\widetilde{C}_0^+(\omega)$ is not shiftable because the assumptions made in the proof of Proposition 1 are valid for $C_0^+(\omega)$, but not for $\widetilde{C}_0^+(\omega)$, an approximation to $C_0^+(\omega)$ [9, Pg.77].

The preceding proposition showed that the non-redundant mapping of an $L^2(\mathbb{R} \to \mathbb{R})$ function approximates the Softy-space image of the low resolution version of the function provided that the function has a lowpass characteristic. Does this assumption really hold for real-world signals and images? When dealing with bandlimited digital signals, we can assume that they have a lowpass characteristic if they are sampled at twice the Nyquist rate. For natural images, it is widely accepted that although these images are usually not bandlimited, they have a lowpass characteristic with low energy in the high-frequency interval [38, Pg. 176]. Having established the importance and applicability of the non-redundant mapping, we shall now describe its properties.

C. The Non-Redundant Mapping: A Realizable Unitary Map

In this section, we shall demonstrate that the non-redundant mapping defines a realizable unitary map between V_1 and $\widetilde{V}_0^+$. To do this we must show that the map $\widetilde{\mathcal{H}}^+$ is linear, realizably bijective and inner-product preserving. The bijectiveness of the map will ensure that the non-redundant mapping is invertible. We shall also prove that the inverse of the non-redundant mapping is realizable with digital filters. This ensures that the non-redundant CWT is practically implementable. It is important to show that the non-redundant mapping preserves inner-products because this allows the non-redundant CWT to be an orthogonal transform, an important requirement in many transform-based signal-processing applications.

Let us now begin the analysis of $\widetilde{\mathcal{H}}^+$. To demonstrate linearity, recall that this map is applied to functions in V_1 by filtering and downsampling the associated scaling-coefficient sequences. Both of these operations are linear. It follows that the non-redundant mapping is also linear. In the next two sub-sections, we demonstrate that $\widetilde{\mathcal{H}}^+$ is a realizable bijection and that it is inner-product preserving.

C.1 The Non-Redundant Mapping: A Realizable Bijective Map

In the following proposition, we prove that the non-redundant mapping is a realizable bijection. This ensures that the mapping has a practical implementation.

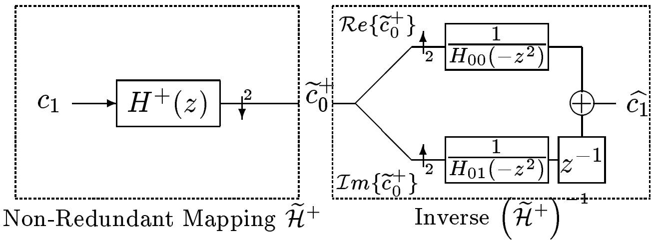

Fig. 13. The non-redundant mapping and its inverse constitute a realizable bijective map because $\hat{c}_1 = c_1$.

Proposition 3: Let h_{00} and h_{01} be real-coefficient, allpass filters selected to be the even- and odd-polyphase components of a lowpass filter h_0. Create a mapping filter h^+ by frequency shifting the lowpass frequency response $H_0(\omega)$ by $\pi/2$, so that $H^+(z) = H_0(-jz)$. Suppose that the scaling-coefficient sequence c_1 is associated with an arbitrary function f_1 in V_1. The "non-redundant mapping" block in Fig. 13 illustrates the forward map $\widetilde{\mathcal{H}}^+$ to the scaling-coefficient sequence $\widetilde{c}_0^+$ associated with the non-redundant mapping $\widetilde{f}_0^+$. The "inverse" block shows the inverse map $(\widetilde{\mathcal{H}}^+)^{-1}$ from $\widetilde{c}_0^+$ to $\hat{c}_1$. Then $\hat{c}_1 = c$, implying that $\widetilde{\mathcal{H}}^+$ is a realizable bijection.

Proof: Selesnick [39] and Phoong et al. [40] describe a design method for the allpass filters h_{00} and h_{01} so that

$$H_0(z) = H_{00}(z^2) + z^{-1} H_{01}(z^2)$$

is indeed a lowpass filter. They also argue that $H_0(z)$ is a root halfband filter that satisfies

$$H_0(z)H_0(z^{-1}) + H_0(-z)H_0(-z^{-1}) = 1.$$

Now, we have $H_{+0}(z) = H_{00}(-z)$ and $H_{+1}(z) = jH_{01}(-z)$, where $H_{+0}(z)$ and $H_{+1}(z)$ are the even- and odd-polyphase components of the mapping filter h_+ that is created from the lowpass filterh_0. If the even- and odd-polyphase components of the scaling-coefficient sequence c_1 are c_{10} and c_{11}, then we can express $\widetilde{C}_0^+(z)$ as

$$\begin{aligned} \widetilde{C}_0^+(z) &= H_{+0}(z)C_{10}(z) + z^{-1}H_{+1}(z)C_{11}(z), \\ &= H_{00}(-z)C_{10}(z) + jz^{-1}H_{01}(-z)C_{11}(z). \end{aligned} \tag{13}$$

By definition, the kernel of the map $\widetilde{\mathcal{H}}^+$ consists of those scaling-coefficient sequences c_1 for which $\widetilde{c}_0^+ = 0$. Therefore, from Equation 13, we deduce that

$$\begin{aligned}\ker(\widetilde{\mathcal{H}}^+) &= \{C_1(z) : H_{00}(-z)C_{10}(z) = -jz^{-1}H_{01}(-z)C_{11}(z)\},\\ &= \{0\},\end{aligned}$$

since c_1 is a real-valued sequence and $H_{00}(-z), H_{01}(-z)$ are real-coefficient allpass filters that are non-zero on the unit circle. We now know that $\widetilde{\mathcal{H}}^+$ is invertible because $\ker(\widetilde{\mathcal{H}}^+) = \{0\}$. The inverse mapping will allow us to reconstruct c_1 from $\widetilde{c}_0^+$. From Equation 13, observe that

$$\begin{aligned}\mathcal{R}e\left\{\widetilde{C}_0^+(z)\right\} &= H_{00}(-z)C_{10}(z),\\ \mathcal{I}m\left\{\widetilde{C}_0^+(z)\right\} &= H_{01}(-z)C_{11}(z),\end{aligned}$$

since c_1 is a real-valued sequence and $H_{00}(-z), H_{01}(-z)$ are real-coefficient filters. Now from Fig. 13, we have

$$\begin{aligned}\hat{C}_1(z) &= \frac{1}{H_{00}(-z)}\mathcal{R}e\left\{\widetilde{C}_0^+(z^2)\right\} + z^{-1}\frac{1}{H_{01}(-z)}\mathcal{I}m\left\{\widetilde{C}_0^+(z^2)\right\}, \qquad (14)\\ &= \frac{1}{H_{00}(-z^2)}H_{00}(-z^2)C_{10}(z^2) + z^{-1}\frac{1}{H_{01}(-z^2)}H_{01}(-z^2)C_{11}(z^2),\\ &= C_{10}(z^2) + z^{-1}C_{11}(z^2),\\ &= C_1(z).\end{aligned}$$

Hence $\hat{c}_1 = c_1$. We conclude by emphasizing that the inverse map $(\widetilde{\mathcal{H}}^+)^{-1}$ is indeed realizable since

$$\begin{aligned}\frac{1}{H_{00}(-z)} &= H_{00}(-z^{-1}),\\ \frac{1}{H_{01}(-z)} &= H_{01}(-z^{-1}),\end{aligned}$$

because $H_{00}(-z), H_{01}(-z)$ are allpass filters. $\square$

The above proposition proves that the forward and inverse maps of Fig. 13 implement the non-redundant mapping $\widetilde{\mathcal{H}}^+$ and its inverse $(\widetilde{\mathcal{H}}^+)^{-1}$ on the scaling-coefficient sequences associated with V_1 functions. Hence $\widetilde{\mathcal{H}}^+$ is a realizable bijective map. Next, we shall consider the preservation of inner-products by the realizable, linear, bijective map $\widetilde{\mathcal{H}}^+$.

C.2 Preservation of Inner Products

Having shown the non-redundant mapping to be linear and realizably bijective, we now complete the demonstration of its unitarity by showing that it preserves the Softy-space inner product.

The preservation of inner products is an important property because it allows the non-redundant CWT to be an orthogonal transform, if an orthogonal DWT is used to compute the DWT of the non-redundant mapping. In Section IV-B, we showed that although Hardy-space mappings and Softy-space mappings preserve the norm induced by the $L^2(\mathbb{R} \to \mathbb{C})$ inner product, they do no preserve the $L^2(\mathbb{R} \to \mathbb{C})$ inner product itself. Consequently, we defined the Softy-space inner product so as to obtain an equivalent inner product that is preserved by Hardy-space mappings and Softy-space mappings. The identical situation arises for the non-redundant mapping. In [9, Pg.81], we prove that the non-redundant mapping does not preserve the $L^2(\mathbb{R} \to \mathbb{C})$ inner product. Then, in [9, Pg.83], we show that the non-redundant mapping preserves the norm induced by the $L^2(\mathbb{R} \to \mathbb{C})$ inner product. Finally, in [9, Pg.85], we prove that the non-redundant mapping preserves the Softy-space inner product, iff h_0 is the sum of allpass polyphase components as described in Proposition 3. This concludes the demonstration of the unitarity of the non-redundant mapping.

D. The Non-Redundant CWT

Now that we have defined the non-redundant mapping and examined its properties, we are ready to introduce the non-redundant CWT. We refer the reader to Figure 14. The non-

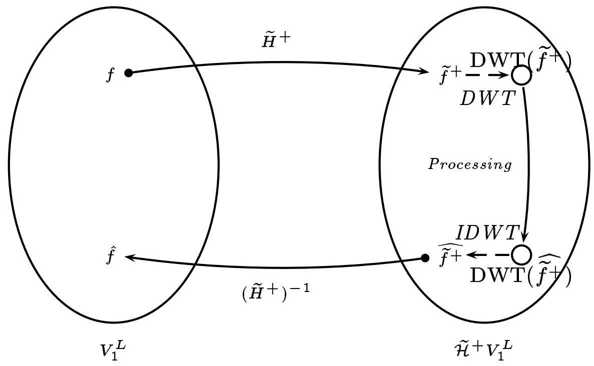

Fig. 14. $\widetilde{f}^+$ is the non-redundant mapping of f and DWT$(\widetilde{f}^+)$ is the non-redundant CWT of f.

redundant mapping $\widetilde{\mathcal{H}}^+$ maps $f \in V_1^L$ to $\widetilde{f}^+ \in \widetilde{\mathcal{H}}^+V_1^L$. The non-redundant CWT consists of the DWT of $\widetilde{f}^+$ and is represented by DWT$(\widetilde{f}^+)$ in the figure. We may perform application-dependent processing of the non-redundant CWT coefficients to obtain DWT$(\widehat{\widetilde{f}^+})$. The inverse DWT yields $\widehat{\widetilde{f}^+}$, the non-redundant mapping of the processed function $\widehat{f}$. To recover $\widehat{f}$, perform the inverse map $(\widetilde{\mathcal{H}}^+)^{-1}$ on $\widehat{\widetilde{f}^+}$. From Proposition 2 and Figure 12 recall that $\widetilde{\mathcal{H}}^+V_1^L$

approximates V_0^{L+}, the Softy-space mapping of V_0^L, a low-resolution version of V_1^L. Therefore, as explained in Section V-B, DWT($\tilde{f}^+$), the non-redundant CWT of f enjoys some of the advantages associated with DWT(f^+), the CWT of f in Figure 4.

In Section V-C.2, we explained that the non-redundant mapping preserves the norm and the Softy-space inner product iff the mapping filter used to implement the mapping is created from a lowpass filter that is the sum of allpass polyphase components. Since a non-trivial allpass filter has an infinite-length impulse response, such a mapping filter will be an IIR filter. Allpass polyphase filters of the type described in the above proposition have also been applied to subband image coding by Smith and Eddins [41]. They stress the implementation efficiency and excellent frequency-response characteristics of these filters. However, for applications in which IIR filters are undesirable, we consider the consequences of FIR approximation to IIR mapping filters in [9, Section 4.4].

VI. Discussion and Conclusion

The DWT is seriously disadvantaged by its shift sensitivity, poor directionality and lack of phase information. In Section I we investigated several different techniques for the mitigation of DWT disadvantages. Most methods address only one of the three drawbacks described above. Notable exceptions are the Complex Steerable Pyramid (CSP) and the Dual Tree Wavelet Transform (DTWT); both transforms overcome all three shortcomings: shift sensitivity, poor directionality and absence of phase information. The CSP uses a non-separable, highly redundant implementation to mitigate DWT disadvantages. However, the overwhelming 3D CSP redundancy of 39 [35] prohibits its usage in data-intensive applications such as seismic signal processing. Moreover, the spatial-domain CSP implementation lacks perfect reconstruction, an important requirement for most signal processing applications. On the other hand, the separable m-dimensional DTWT has a lower redundancy of 2^m, is perfectly reconstructing and also overcomes all DWT shortcomings. This transform has been used in various applications with excellent results. To obtain perfect reconstruction, the DTWT uses real-coefficient filters in two DWT trees. Conceptually however, the DTWT coefficients may be obtained using a DWT with quasi-analytic filters. This quasi-analytic filter decomposition enables the mitigation of all three DWT disadvantages.

The central concept in this paper is that the analytic-filter DWT decomposition of a real signal is equivalent to the real-filter DWT decomposition of the Hardy-space mapping of the signal. Therefore, DTWT-like properties are attainable using *any* DWT preceded by a mapping onto Hardy space. Our mapping-based approach has two advantages over the DTWT: first, the flexibility to use an arbitrary DWT decomposition; and second, the ability to control transform redundancy.

The flexibility to use an arbitrary DWT in our mapping-based approach arises from the decoupling in its implementation. Whereas the DTWT implementation requires the joint design of a quadrature-pair of wavelets, our mapping-based approach consists simply of a mapping stage followed by a DWT stage. This decoupling into two stages allows for the flexibility to use any arbitrary DWT decomposition. In [9], [10] we show how this flexibility can be exploited, for example, to create the Complex Double-density DWT (CDDWT): a shift-insensitive, directional, complex wavelet transform with a low-redundancy of $\frac{3^m-1}{2^m-1}$ in m dimensions. To the best of our knowledge, no other transform achieves all these properties at a redundancy that is lower than $\frac{3^m-1}{2^m-1}$. In [9, Chapter 7], [10], we demonstrate persuasively that the CWT and the CDDWT achieve state-of-the-art results in 2D and 3D seismic signal processing applications. We expect that these transforms may also be used for the same applications in which the DTWT has yielded excellent results.

The ability to control the transform redundancy of our mapping-based approach arises from the controllability of the redundancy in the mapping stage. The decoupling in the implementation of our mapping-based approach implies that transform redundancy is determined by the mapping step. Consequently, by creating a non-redundant mapping stage, we obtain a directional, non-redundant, complex wavelet transform: the non-redundant CWT. To the best of our knowledge, no other complex wavelet transform is simultaneously directional and non-redundant. These properties make the non-redundant CWT particularly attractive for use in image-coding systems. Reeves and Kingsbury [42], Portilla and Simoncelli [36], and Romberg et al. [33], have derived accurate statistical models for complex wavelet coefficients. These models have proven useful in various different signal-processing applications. However, none of these models may be used for image coding, due to the redundancy of the transforms on which the models are based. On the other hand, because it can exploit directionality and statistical complex-wavelet models in a non-redundant framework, the non-redundant complex-wavelet transform has significant potential benefits for image coding systems.

We have shown that our mapping-based framework for complex wavelet transforms mitigates

DWT shortcomings and provides important advantages that engender new complex wavelet transforms with unprecedented properties. In theory, the mapping stage must map a real input signal onto the Hardy space $H^2(\mathbb{R} \to \mathbb{C})$; in practice, such a mapping is unrealizable. To circumvent this obstacle, we defined a new function space, the Softy space S^+. We accomplish the mapping onto Softy space by using a digital mapping filter h^+. We proved that the Softy space S^+ is isomorphic and approximately equal to the Hardy space $H^2(\mathbb{R} \to \mathbb{C})$. For applications in which non-redundancy is critical, we control the redundancy of the mapping-stage by defining a non-redundant mapping. This mapping stage introduces no redundancy into the transform. We proved that the non-redundant mapping of a real signal approximates its Softy-space mapping, provided that the signal has a lowpass characteristic. We also demonstrated that the non-redundant mapping is a realizable, unitary map. We defined the non-redundant CWT to be the DWT of the non-redundant mapping of an $L^2(\mathbb{R} \to \mathbb{R})$ function. In [9], [10] we explain how the non-redundant CWT provides excellent results in seismic signal-processing applications.

To conclude, we emphasize that our new framework for mapping-based CWTs not only overcomes serious DWT disadvantages but also offers the additional benefits of controllable redundancy and flexibility. These benefits allow for the creation of new transforms with significant advantages for a variety of applications. In particular, applications such as image coding in which non-redundancy is critical may now benefit from complex-valued wavelet coefficients.

References

[1] I. Daubechies, "Orthonormal bases of compactly supported wavelets," *Comm. Pure Applied Math.*, vol. XLI, no. 41, pp. 909–996, Nov. 1988.

[2] G. Strang and T. Nguyen, *Wavelets and Filter Banks*, Wellesley-Cambridge Press, Wellesley, MA, 1996.

[3] C. S. Burrus, R. A. Gopinath, and H. Guo, *Introduction to Wavelets and the Wavelet Transform - A Primer*, Prentice-Hall, 1998, Expansion of notes for the IEEE Signal Processing Society's tutorial program held in conjunction with the ICASSP-93 on April 26, 1993.

[4] G. Strang, "Wavelets and dilation equations: A brief introduction," *SIAM Review*, vol. 31, no. 4, pp. 614–627, 1989, also, MIT Numerical Analysis Report 89-9, August 1989.

[5] A. Watson and J. A. J. Ahumada, "Model of human visual-motion sensing," *Journal of Optical Society of America*, vol. 2, no. 2, pp. 322–342, 1985.

[6] T. Burns, S. Rogers, D. Ruck, and M. Oxley, "Discrete, spatiotemporal, wavelet multiresolution analysis method for computing optical flow," *Optical Engineering*, vol. 33, no. 7, pp. 2236–2247, 1994.

[7] A. Grossman, R. Kronland-Martinet, and J. Morlet, "Reading and understanding continuous wavelet transforms," in *Wavelets Time-Frequency Methods and Phase Space*, J. M. Combes, A. Grossman, and Ph.

Tchamitchian, Eds., Berlin, 1989, pp. 2–20, Springer-Verlag, Proceedings of International Colloquium on Wavelets and Applications, Marseille, France, December 1987.

[8] A. Grossman and J. Morlet, "Decomposition of hardy functions into square integrable wavelets of constant shape," *SIAM J. Math. Anal.*, vol. 15, no. 4, pp. 723–736, 1984.

[9] F. C. A. Fernandes, *Directional, Shift-Insensitive, Complex Wavelet Transforms with Controllable Redundancy*, Ph.D. thesis, Rice University, Jan. 2002, http://www.ece.rice.edu/-felixf/dissertation.pdf.

[10] F. C. A. Fernandes, R. L. C. van Spaendonck, and C. S. Burrus, "Multi-dimensional, mapping-based complex wavelet transforms," In preparation for submission to IEEE Transactions on Image Processing, 2002.

[11] S. Mallat, "Zero-crossings of a wavelet transform," *IEEE Trans. Inform. Theory*, vol. 37, no. 4, July 1991.

[12] G. Beylkin, "On the representation of operators in bases of compactly supported wavelets," *SIAM J. Numer. Anal.*, vol. 29, no. 6, pp. 1716–1740, 1992.

[13] R. R. Coifman and D. L. Donoho, "Translation-invariant de-noising," Tech. Rep., Stanford University, Department of Statistics, 1995, To Appear, Wavelets and Statistics, Anestis Antoniadis, ed. Springer-Verlag Lecture Notes.

[14] H. Guo, "Theory and applications of the shift-invariant, time-varying and undecimated wavelet transform," M.S. thesis, Rice University, Houston, TX, May 1995.

[15] M. Lang, H. Guo, J. E. Odegard, C. S. Burrus, and R. O. Wells, Jr., "Noise reduction using an undecimated discrete wavelet transform," *IEEE Signal Processing Letters*, vol. 3, no. 1, pp. 10–12, Jan. 1996, Also Tech. report CML TR95-06.

[16] J. Liang and T. W. Parks, "A translation invariant wavelet representation algorithm with applications," *IEEE Trans. SP*, vol. 44, no. 2, pp. 225–232, Feb. 1996.

[17] S. A. Benno and J. M. F. Moura, "Scaling functions robust to translations," *IEEE Transactions on Signal Processing*, vol. 46, no. 12, pp. 3269–3281, Dec. 1998.

[18] F. Bao and N. Erdol, "The optimal wavelet transform and translation invariance," in *IEEE Proc. Int. Conf. Acoust., Speech, Signal Processing*, 1994, vol. 3, pp. 13–16.

[19] I. W. Selesnick, "The double density DWT," in *Wavelets in Signal and Image Analysis: From Theory to Practice*, A. Petrosian and F. G. Meyer, Eds. Kluwer, 2001.

[20] E. P. Simoncelli, W. T. Freeman, E. H. Adelson, and D. J. Heeger, "Shiftable multi-scale transforms," *IEEE Trans. Inform. Theory*, vol. 38, no. 2, pp. 587–607, Mar. 1992.

[21] Q. Wang and L. Wu, "A unified approach to translation-invariance problem," Preprint, 1998.

[22] P. Abry, *Transformées en ondelettes – Analyses multirésolution et signaux de pression en turbulence*, Ph.D. thesis, l'Universite Claude Bernard - Lyon I, 1994.

[23] J. Magarey, *Motion estimation using complex wavelets*, Ph.D. thesis, University of Cambridge, 1997.

[24] N. G. Kingsbury and J. F. A. Magarey, "Wavelet transforms in image processing," in *Proc. First European Conference on Signal Analysis and Prediction*, Prague, June 24-27 1997, pp. 23–34.

[25] N. Kingsbury, "Image processing with complex wavelets," *Phil. Trans. R. Soc. Lond.*, Sept. 1999.

[26] I. Selesnick, "The design of Hilbert transform pairs of wavelet bases," *IEEE Transactions on Signal Processing*, May 2002.

[27] I. W. Selesnick, "Hilbert transform pairs of wavelet bases," *IEEE Signal Processing Letters*, vol. 8, no. 6, June 2001.

[28] R. A. Gopinath, "The phaselet transform - an integral redundancy nearly shift-invariant wavelet transform," Preprint, Nov. 2001.

[29] R. H. Bamberger and M. J. T. Smith, "A filter bank for the directional decomposition of images: Theory and design," *IEEE Transactions on Signal Processing*, vol. 40, no. 4, pp. 882–893, Apr. 1992.

[30] D. L. Donoho and M. R. Duncan, "Digital curvelet transform: Strategy, implementation and experiments," in *Proceedings of SPIE, Wavelet Applications VII*, 2000, vol. 4056.

[31] E. Candès and D. Donoho, "Curvelets," Manuscript, 1999.

[32] M. Do and M. Vetterli, "Pyramidal directional filter banks and curvelets," in *IEEE Proc. Int. Conf. Image Processing*, 2001.

[33] J. K. Romberg, H. Choi, R. G. Baraniuk, and N. G. Kingsbury, "Hidden Markov tree models for complex wavelet transforms," *IEEE Transactions on Signal Processing*, 2001 (submitted).

[34] J. Romberg, H. Choi, and R.G.Baraniuk, "Multiscale edge grammars for complex wavelet transforms," in *IEEE Proc. Int. Conf. Image Processing*, Thessaloniki, Greece, 2001.

[35] R. van Spaendonck and R. G. Baraniuk, "Directional scale analysis for seismic interpretation," in *Annual Meeting Abstracts*. 1999, pp. 1844–1847, Society Of Exploration Geophysicists.

[36] J. Portilla and E. P. Simoncelli, "A parametric texture model based on joint statistics of complex wavelet coefficients," *International Journal of Computer Vision*, 2000.

[37] F. G. Meyer and R. R. Coifman, "Brushlets: a tool for directional image analysis and image compression," *Applied and Computational Harmonic Analysis*, vol. 4, pp. 147–187, 1997.

[38] G. H. Granlund and H. Knutsson, *Signal Processing for Computer Vision*, Kluwer Academic Publishers, 1995.

[39] I. W. Selesnick, "Lowpass filters realizable as allpass sums: design via a new flat delay filter," *IEEE Trans. on Circuits and Systems Part II*, vol. 46, no. 1, pp. 40–50, Jan. 1999.

[40] S.-M. Phoong, C.W. Kim, P.P. Vaidyanathan, and R. Ansari, "A new class of two-channel biorthogonal filter banks and wavelet bases," *IEEE Trans. SP*, vol. 43, no. 3, pp. 649–665, Mar. 1995.

[41] M. J. T. Smith and S. L. Eddins, "Analysis/synthesis techniques for subband image coding," *IEEE Transactions on Acoustics, Speech, and Signal Processing*, vol. 38, no. 8, pp. 1446–1456, Aug. 1990.

[42] T. H. Reeves and N. G. Kingsbury, "Prediction of coefficients from coarse to fine scales in the complex wavelet transform," in *IEEE Proc. Int. Conf. Acoust., Speech, Signal Processing*, 2000.